Eur. Phys. J. D **28**, 219–228 (2004)
DOI: 10.1140/epjd/e2003-00314-3

THE EUROPEAN PHYSICAL JOURNAL D

Rearrangement collisions between gold clusters*

J. Rogan[1], R. Ramírez[2], A.H. Romero[2,3], and M. Kiwi[2,a]

[1] Departamento de Física, Facultad de Ciencias, Universidad de Chile, Casilla 653, Santiago 1, Chile
[2] Facultad de Física, Universidad Católica de Chile, Casilla 306, Santiago, Chile 6904411
[3] Advanced Materials Department, IPICyT, Apartado Postal 3-74 Tangamanga, 78231 San Luis Potosí, SLP México, Mexico

Received 16 July 2002 / Received in final form 19 May 2003
Published online 23 December 2003 –

Abstract. Collision processes between two gold clusters are investigated using classical molecular dynamics in combination with embedded atom (EA) potentials, after checking the reliability of the EA results by contrasting them with first principles calculations. The Au projectiles considered are both single atoms ($N = 1$) and clusters of $N = 2$, 12, 13 and 14 atoms. The targets contain $N = 12$, 13 and 14 gold atoms. The collision energy E and impact parameter b are chosen within a range such that the three regimes we are interested in studying (fusion, scattering and fragmentation) are realized. The results of the collision processes are described and analyzed in detail, and compared with previous work.

PACS. 36.40.Qv Stability and fragmentation of clusters – 36.40.Mr Spectroscopy and geometrical structure of clusters – 61.46.+w Nanoscale materials: clusters, nanoparticles, nanotubes, and nanocrystals – 82.30.Nr Association, addition, insertion, cluster formation

1 Introduction

Gold undoubtedly is, and has been, an important material to mankind, both in everyday life and in scientific endeavors. Gold clusters have been used for centuries in colloidal suspension (to stain glass) and recently as catalysts in the selective CO oxidation [1]. On the other hand, the study of nanostructures has recently attracted widespread interest among theoretical and experimental physicists and chemists, and because of its many applications has also come to the forefront of technology [2]. On the theoretical side ab initio procedures are now capable of providing incisive insights into the properties of these systems. In addition, novel and sophisticated nanostructure fabrication, manipulation and measurement techniques have given impetus to experiment, and reliability to a large amount of experimental data [3–8]. Moreover, the technological applications on a variety of devices has strongly stimulated activity in the nanostructure field since they can be used as building blocks of novel nanostructured materials and devices [9–12].

In particular, metallic clusters provide an interesting subject of study for at least three reasons: (i) clusters constitute intermediate systems between isolated atoms and molecules, on the one extreme, and bulk solids on the other (i.e. they constitute genuine mesoscopic systems); (ii) they have a large ratio of surface to volume atoms; and (iii) they often exhibit an interesting phenomenology of their own. Gold clusters have received widespread attention during the last two decades, both experimentally [3–8] and theoretically [13–26]. Quite recently Li et al. [27], based on results obtained by photoelectron spectroscopy, carried out a relativistic DFT calculation that suggests that Au_{20} possesses a tetrahedral structure, which is a fragment of the gold bulk fcc one with a slight relaxation, but with properties that differ markedly from bulk gold.

In principle one does expect ab initio procedures to be the definitive tool to handle this type of cluster collisions; however, it is not always feasible (or at least practical) to implement such ab initio calculations. Andersen et al. [28–30] not long ago provided an exhaustive review of the literature which covers, among many other topics, ab initio treatments ranging from the simplest case: a proton colliding a hydrogen atom ($H^+ + H$) all the way to strontium collisions with noble gases. However, since we are interested in structures with a fairly large number of atoms, or arranged in several different interacting nanostructures, ab initio computations at first (for small clusters) become very time consuming and in the end (for large clusters), impractical. Much the same happens when attempting to obtain a detailed description of the long time evolution of small systems, or to describe their properties when subject to a variety of external conditions.

The field of cluster-cluster collisions, in the three regimes we are interested in (fusion, scattering and

* Supported by the *Fondo Nacional de Investigaciones Científicas y Tecnológicas* (FONDECYT, Chile) under grants #8990005, #1010988 and 1030957 and DIPUC-Chile.
[a] e-mail: mkiwi@puc.cl

fragmentation) has been very active and fruitful. We mention as examples of this activity several papers that bear a direct relation with the present contribution and which deserve special attention. Schmidt, Seifert, Lutz and collaborators [31–33] thoroughly studied cluster collisions, by MD simulations. In references [31,32] $Na_9 + Na_9$ reactions were simulated using the MD-DFT method. In the former fusion, deep inelastic and quasi-elastic scattering were investigated, while in the latter the electronic structure and energetic stability was clarified. The intercluster potential for $Na_n + Na_n$, with $n = 8$, 9, 19 and 20 was calculated [33]. Transient Na dimer cluster formation was further investigated by Zhang et al. [34] using tight-binding MD. Reviews by Andersen et al. [28–30] examine in great detail the related phenomenon of alignment and orientation effects in cluster-cluster and ion-cluster collisions.

Schmidt and Lutz [35], proposed a classical reaction model to study the fusion and reaction cross-sections of metal-metal cluster collisions, in view of the fact that detailed quantum mechanical calculations are so enormously time consuming. A simple stability condition to attain fusion of atomic clusters, atomic nuclei and liquid droplet collisions was also put forward by the same authors [36]. This model incorporates the concept of maximum angular momentum, which if exceeded leads to instability of the system against centrifugal fragmentation. Metallic and semiconductor cluster fragmentation was also investigated by Mazzone [37] using a semi-empirical quantum mechanical method.

More recently [38] a joint experimental and theoretical effort succeeded in developing a better understanding of collisions of rather large and complex systems, such as $C_{60}^+ + C_{60}$. In the experiments a C_{60}^+ ion beam was targeted on a chamber containing neutral fullerenes heated to around 450 °C. The results were compared with quantum molecular dynamics calculations and the fusion model mentioned above [36]. Also other sophisticated experimental efforts have recently been setup. Quite recently Campbell et al. [39] reported an experimental study accompanied by theoretical interpretation of cluster-cluster fusion and fragmentation. A good understanding of the $C_{60}^+ + C_{70}$ (or $C_{70}^+ + C_{60}$) and $C_{70}^+ + C_{70}$ was developed. However, the same success was not achieved for the $C_{60}^+ + C_{60}$ process. Schweikhard's group [40,41] achieved a model free determination of dissociation energies of ionized polyatomic gold clusters (Au_n^+), which are in semi-quantitative agreement with our computed estimates, as will be seen below.

On the other hand, more than a decade ago the bombardment with gold clusters of metallic surfaces was investigated experimentally [42] and theoretically [43–45]. Moreover, the dramatic energy accommodation that occurs in cluster-cluster collisions, which is crucial to understand the growth mechanism during the early stages of particle formation, was investigated around the same time by Blastein et al. [46].

Here we intend to develop an adequate description of colliding gold clusters, a phenomenon which falls into one or more of the categories described in the preceding paragraphs. From an historical, technological and basic science point of view gold is an interesting material by itself. It corresponds to atomic number 79 in the Periodic Table and has a rather large mass (197). Since, in addition to the characteristics already mentioned gold is a metal, an ab initio description of gold cluster-cluster collisions is not feasible at this time. Thus we carried out a systematic MD study of Au + Au collisions, for which the energy E and impact parameter b are chosen in such a way that the three regimes we are interested in studying, that is: fusion, scattering and fragmentation, are realized. The impact parameter b is varied between 0 (head-on collision) and 7 Å and the projectile energy $0 \leq E \leq 1.5$ eV per atom. The maximum energy $E = 1.5$ eV per atom corresponds to approximately one half of the binding energy of the cluster.

In this paper we employ mainly classical molecular dynamics, an alternative to the ab initio computation scheme that has proven to be quite reliable [21]. Classical molecular dynamics (MD) is a valid option in this case, since it allows to considerably reduce the computation time (relative to ab initio MD calculations), and/or to increase substantially the number of particles that can be handled. Obviously, there is a price to pay; as examples of this cost we mention that the method is at best semi-classical, that the detailed electronic structure is ignored, and that phenomenological potentials, adjusted to fit bulk properties, are used.

In spite of these shortcomings the MD technique can reliably be used to compute the properties dominated by the ionic contribution, which is the case for the phenomena treated in this paper. This is especially true when MD is checked, in some physical limit, against first principle calculations. An alternative, but equally convenient procedure, is to close in on a solution, for example for geometrical optimization via MD, to be followed by first principle calculations. The synergy between ab initio and MD thus allows to significantly reduce the resources that are required and to expand the set of problems amenable to treatment. Precisely this synergy has been used to investigate the fusion cross-section of fullerenes [47].

We focus our interest on the dynamics of gold cluster collisions. In particular we study the structure and symmetry of small Au clusters, and the dynamics of atom–cluster and cluster–cluster collisions, for different values of the impact parameter b and of the center of mass energy E.

This paper is organized as follows: after this introduction we describe, in Section 2, both the ab initio and EA methods employed in the computations. In Section 3 we provide results, for a large variety of cases, of the implementation of the codes, for the cluster structures, their symmetries and the dynamics of the collision process. Finally, in Section 4 we draw conclusions and close the paper.

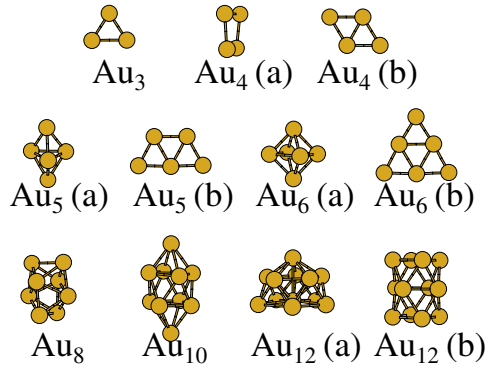

Fig. 1. Ab initio optimized geometries for 3, 4, 5, 6, 8, 10 and 12 atom gold clusters.

2 Simulation method

2.1 Ab initio method

In order to assess the quality of the semi-empirical embedded atom (EA) procedure used in the context of our classical molecular dynamics simulations, we start contrasting EA against first principles calculations. Thus, ab initio geometrical optimization was carried out within the Car-Parinello approach [48], in the framework of the density functional theory, using gradient corrections in the PBE implementation [49]. Gradient corrected functionals have been adopted in recent theoretical studies of geometrical optimization of metallic clusters, mainly because they are more accurate than the local density functional, even though there still is some controversy in the literature on the ground state geometry of small Au clusters [16,50,51]. We have obtained [52] some preliminary ab initio results for the geometries and energies of a number of gold clusters, that contain just a few atoms, which we trust will contribute to clarify some of the controversial geometries. The ab initio calculations reported here were performed at the Γ-point of the Brillouin zone, using norm conserving pseudopotentials [53]. The wavefunctions were expanded in plane waves, with an energy cutoff of 60 Ry. We have explicitly checked that, with this energy cutoff, the structural properties of our system are well converged. The box used in the calculations was always at least three times larger than the cluster diameter. The ab initio optimized geometries are illustrated in Figure 1. These geometries should be contrasted with the EA results illustrated in Figure 2, which were obtained for a much larger number of clusters. We display the ones that range in size from 3 to 26 gold atoms, and as expected, EA does not yield planar structures (except for the trivial 3 atom case), but compares quite well with the available ab initio results for three dimensional structures. A surprising outcome is that the Au_3 cluster obtained via ab initio is an equilateral triangle, while EA yields the experimentally observed isoceles triangle structure.

The results obtained for the binding energy E_b, as well as their EA counterparts, are given in Table 1. While the EA method overbinds the cluster in general the agreement between ab initio, EA and Wilson and Johnston [22] (WJ) procedures is quite satisfactory for large clusters ($N \geq 10$) and provides a reasonable basis to trust the EA calculations that constitute the core of the present paper.

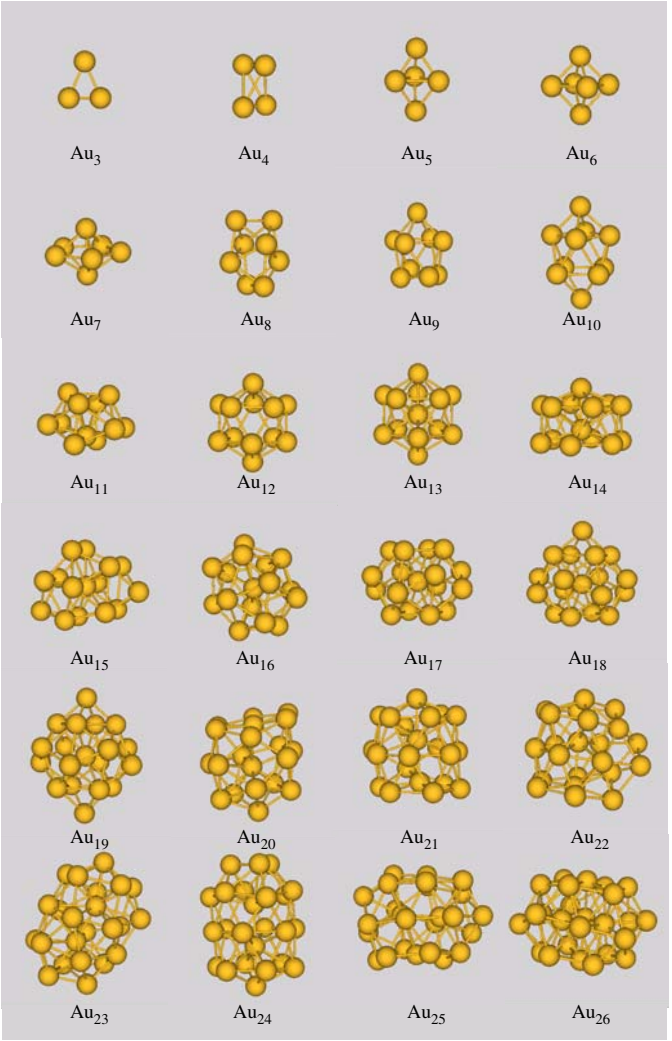

Fig. 2. *Embedded atom* optimized geometries for the clusters considered in this work.

2.2 Embedded atom method

The interatomic interaction between gold atoms is modeled using semi-empirical embedded atom (EA) potentials [54,55]. On the basis of these EA potentials we obtain the average binding energy per atom, E_b, which is later on minimized to yield the optimal cluster geometry. The latter is achieved using a Monte Carlo procedure, for which we adopted as starting configurations, for the different cluster sizes, the geometries obtained by WJ [22] (WJ). Once the optimal geometry is established several static properties, like nearest neighbor distances and angles, and the average coordination number, are readily evaluated.

Table 1. Symmetries, per atom binding energies and average nearest neighbor distances, as computed with different numerical methods.

Cluster	Method	Symmetry	E_b [eV]	R [Å]
3 atoms	EA	C_{2v}	2.405	1.937–2.438
	CP	C_{2v}	0.846	2.350–2.863
	WJ	D_{3h}	1.759	2.780
4 atoms	EA	D_{2d}	2.313	1.904–2.874
	CP (a)	D_{2d}	0.966	2.558–2.865
	CP (b)	D_{2h} (planar)	1.186	2.700
	WJ	T_d	2.178	2.793
5 atoms	EA	O_h	2.685	2.507
	CP (a)	O_h	1.141	2.790
	CP (b)	C_{2v} (planar)	1.317	2.708
	WJ	O_h	2.382	2.801
6 atoms	EA	O_h	2.825	2.536
	CP (a)	O_h	1.207	2.828
	CP (b)	D_{3h} (planar)	1.536	2.708
	WJ	O_h	2.574	2.789
8 atoms	EA	D_{2d}	2.937	2.577
	CP	D_{2d}	1.550	2.816
	WJ	D_{2d}	2.736	2.790
10 atoms	EA	D_{4d}	2.999	2.594
	CP	D_{4d}	1.692	2.904
	WJ	D_{4d}	2.837	2.778
12 atoms	EA (a)	I_h	3.027	2.604
	EA (b)	C_{5v}	3.089	2.693
	CP (a)	C_{5v}	1.588	2.898
	CP (b)	D_{4h}	1.662	2.873
	WJ	I_h	2.886	2.776

After the various different clusters are properly characterized we use classical molecular dynamics (MD) to simulate the cluster–cluster collision process. Many body EA semi-empirical potentials are used throughout. To integrate the equations of motion we implement the Verlet velocity algorithm, with a 1 femtosecond time step. Since the collision fragments heat up as a consequence of the collision process it is necessary to cool them to room temperature; we do so rescaling the temperature under the assumption that the excess energy is released, first by fragmentation and afterwards by radiation. Thus, we rescale the temperature according to a Wien-like σT^4 law, to reach room temperature (300 K) by slow quenching, in which we have taken the σ prefactor of Wien's law much larger than its actual value, because of computer time limitations. In fact we carry out the slow quenching procedure in 10^6 time steps. In some cases, which will be specified below, we allow for three different alternative temperature schedules; we allow the system to evolve in time without cooling for 10^4, 10^6 and 2×10^6 time steps before slow quenching, in order to simulate a competition between the two cluster cooling mechanisms: fragmentation and heat radiation. Finally, the collision fragments are carefully scrutinized to extract the physical information we are seeking.

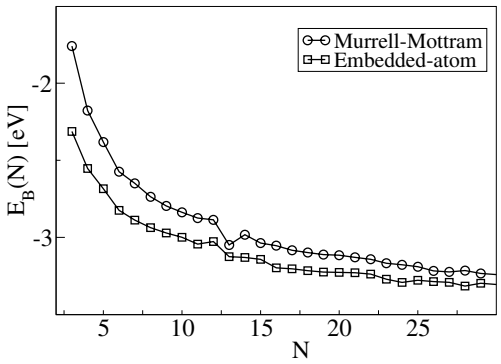

Fig. 3. Binding energies per atom E_b, obtained by WJ using the Murrell–Mottram potential, and by us on the basis of the EA potential, as a function of the number of atoms in the cluster N. The ab initio results, for which we have considered several possible geometries, are detailed in Table 1.

3 Results and discussion

3.1 Structures

The first issue we address is to check the reliability of our MD procedure as compared with alternative methods. In Table 1 we compare the average binding energy E_b of the lowest energy configurations, and the average nearest neighbor distance R, of clusters built with different numbers of gold atoms. On the one hand we have ab initio results obtained within the framework of density functional theory, and on the other the empirical potential results of WJ [22] (who used the Murrell–Mottram [56,57] potential) as well as the EA values that we obtained.

It is quite apparent that the EA overestimates the values of E_b, which differ considerably from the ones found by WJ, and also with the more trustworthy ab initio results. However for small clusters the geometrical parameters are not so satisfactory. This small N (where N is the number of atoms in the cluster) error margin is not surprising, since the EA potential has been adjusted to fit bulk properties and cannot be expected to fully succeed in systems where N is tiny. However, and also as expected, the situation improves as N increases, which is precisely what is borne out by Table 1, where we display results for the range of clusters sizes from $N = 3$ to 12. The same trend is observed in Figure 3, where we plot E_b versus N. Ab initio calculations were performed for $N = 4$, 5 and 6 planar and three dimensional structures (see Tab. 1). It is apparent that as the cluster size increases, specially when the number of atoms is larger than 10, that both the ab initio and EA values tend towards the bulk value. Moreover, these binding energies are in qualitative agreement with the fragmentation energies obtained by Walther et al. [58] for Au_{15}^+, and with dissociation energies computed recently

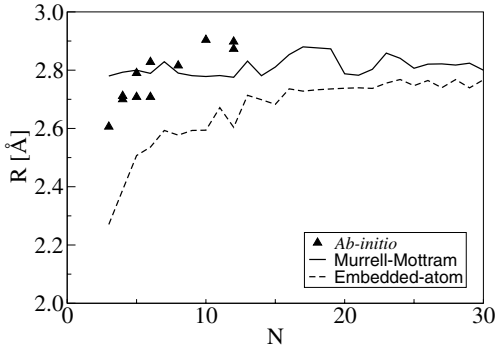

Fig. 4. Average nearest neighbor distances R calculated ab initio (full triangles), using EA (dashed line), and those obtained by WJ using the Murrel-Mottram potential (full line).

by Vogel et al. [40] for Au_{17}^{+} using RRK [59], QRRK [60], RRKM [61] and Weisskopf [62] formulas.

The average nearest neighbor distances R that we compute also exhibit larger errors than those of WJ. In spite of the fact that we employ the WJ cluster configurations as the starting point for our calculations, but in which we use a binding energy obtained from a different potential, we derive geometrical structures which differ from those of WJ. However, once again, increasing N yields compatible results. For example, for a 3-atom cluster the difference in nearest neighbor distances amounts to 15%, but already for a 6-atom cluster it reduces to only 8%. These average distances are illustrated in Figure 4, where we plot R as a function of the number of atoms in the cluster, N. In contrast with Figure 3 the plot of Figure 4 is not smooth, but shows abrupt variations between two successive values of N. Despite this roughness the tendency of the WJ and our EA plots is to approach each other in the large cluster limit. Moreover, our results are in good agreement with the ab initio ones obtained by Wang [17].

3.2 Symmetries

In addition to the binding energies and interatomic distances the cluster symmetry is a relevant characteristic and, in the context of gold cluster topologies, the Jahn-Teller effect is also an important element. Ab initio calculations predict a C_{2v} symmetry for Au_3 and Au_4, while EA yields C_{2v} and D_{2d}, and the Murrell–Mottram potential used by WJ yields D_{3h} and T_d symmetries, respectively. These differences are observed in the pair correlation function $g(r)$ plotted in Figure 5, where it is apparent that the Murrel-Mottram potential yields a much sharper nearest neighbor peak, located farther apart than the one obtained by the EA method.

The second difference in the binding energy is defined by

$$\Delta_2 E_b(N) = 2E_b(N) - E_b(N-1) - E_b(N+1), \qquad (1)$$

and gives an indication of the stability of a cluster with respect to disproportionation [2], as well as its ionic hardness. A plot of $\Delta_2 E_b(N)$ as a function of N is given in

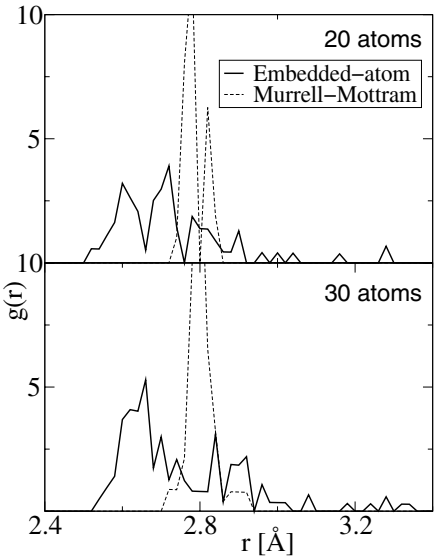

Fig. 5. Pair correlation function $g(r)$ for 20 and 30 Au atom clusters as calculated by us, using EA potentials, and by WJ.

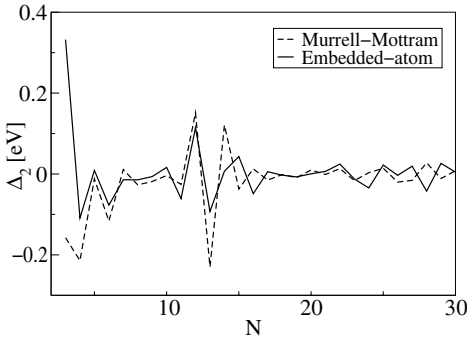

Fig. 6. Second difference in the binding energy $\Delta_2 E_b(N)$ as a function of cluster size N.

Figure 6, where we observe a good agreement of our EA values with those reported by WJ [22], both for the position and magnitude of the hardness peaks. The maxima (minima) of $\Delta_2 E_b(N)$ imply that there are values for which it is more difficult (easier) to add an atom to the cluster. Moreover, as N grows the plot becomes quite smooth, which constitutes an indication that the cluster can incorporate an additional atom without major hindrance.

3.3 Collisions between a single Au atom and a Au cluster

Next we report the results of our simulations of the collisions between a single Au atom and a variable size Au cluster, for several values both of the initial per atom energy E and of the impact parameter b. The precise details that describe the collision process are as follows: at time $t = 0$ the centers of mass of the atom and the cluster are displaced, parallel to the x-axis, ± 10 Å away from the origin, respectively, with the cluster at ($x = 10$, $y = 0$) and the atom located a distance b away from the x-axis,

at ($x = -10$, $y = b$), all on the xy-plane. The principal symmetry axes of the various clusters are aligned perpendicular to the direction of motion, that is parallel to y. The impact parameter b is varied between 0 (head-on collision) and 7 Å; the latter corresponds to the distance where the interaction potential effectively vanishes, since the average radius of a cluster with $12 \leq N \leq 14$ is less than 3 Å and the interaction is cut off at 5.5 Å. The projectile energy is varied between 0.1 and 1.5 eV per atom, in steps of 0.2 eV (8 values in all). The maximum energy $E = 1.5$ eV per atom corresponds to approximately one half of the cluster binding energy. In this way the three regimes we are interested in (fusion, scattering and fragmentation) are achieved. After the collision takes place the resulting fragments are stabilized, by gradual cooling (slow quenching) of the internal velocities. Finally, we analyze the data characterizing the collision fragments for several special cases.

We consider two categories: (i) the scattering of a single gold atom against clusters with $N = 12$, 13 and 14 atoms, which is dealt with here; and, (ii) the scattering of a variable size projectile ($N = 12$, 13 and 14) on a variable size target with a similar number of Au atoms, which is presented in Section 3.4. Throughout we use the concepts of low and high energies, and small and large impact parameters. Low energies are defined to be in the range $0.1 \leq E \leq 0.7$ eV and large within $0.8 \leq E \leq 1.5$ eV. Similarly, small impact parameters cover the range $0 \leq b \leq 3$ Å, and large is defined as $4 \leq b \leq 7$ Å. The upper bounds on E and b, as mentioned above, are related to the binding energy of the cluster and the distance at which the projectile does not interact with the target, respectively.

One atom on 12. Because of the rich variety of results, and to facilitate their understanding by the reader, we have chosen to illustrate them by means of figures. In particular Figure 7 describes the one gold atom collision with a 12 atom cluster. In Figure 7 we illustrate the results of three different temperature reducing schedules. The upper table corresponds to allowing the system to evolve at constant temperature for 10^4 time steps *before* starting a 10^6 time steps long radiation cooling process. In this and ensuing figures the columns correspond to different values of the energy per atom (in eV), while the rows correspond to several different impact parameters in Å units. Each entry characterizes a collision on the basis of the following symbols: single atoms, dimers and trimers are represented by a dot, two dots joined by a line, and three dots that form a triangle, respectively. When several of these collision fragments are generated we denote their number by a factor in front of the corresponding symbol. If the fragment contains four or more atoms the symbolic representation is a circle. Finally, if the number of atoms in the target is not altered after the collision, we stress this fact representing it by a square with the original number of target atoms in its interior, as long as $N \geq 4$.

It is noticed that for low energy and small impact parameter ($0 \leq b \leq 3$ Å), projectile and target fuse into a 13 atom cluster. When the energy is increased to

	0.1	0.3	0.5	0.7	0.9	1.1	1.3	1.5
0	⑬	⑬	⑬	⑬	⑬	⑬	⑪ 1	⑪ 1
1	⑬	⑬	⑬	⑬	⑬	⑪ 1	⑪ 1	⑬
2	⑬	⑬	⑬	⑬	⑬	⑬	⑪ 1	⑬
3	⑬	⑬	⑬	⑬	⑬	⑪ 1	⑪ 1	⑪ 1
4	⑬	⑬	⑬	⑬	⑬	⑪ 1	⑬	⑪ 1
5	⑬	⑬	⑬	[12] 1•	[12] 1•	[12] 1•	[12] 1•	[12] 1•
6	⑬	⑬	⑬	⑪ 1	⑬	⑬	[12] 1•	[12] 1•
7	⑬	⑬	[12] 1•	[12] 1•	[12] 1•	[12] 1•	[12] 1•	[12] 1•

	0.1	0.3	0.5	0.7	0.9	1.1	1.3	1.5
0	⑬	⑬	⑬	⑪ 1	⑨ 2	⑨ 2	⑦ 3	⑤ 4
1	⑬	⑪ 1	⑬	⑨ 2	⑨ 2	⑨ 2	⑨ 2	⑦ 3
2	⑬	⑬	⑪ 1	⑪ 1	⑪ 1	⑨ 2	⑨ 2	⑦ 3
3	⑬	⑬	⑪ 1	⑪ 1	⑨ 2	⑪ 1	⑪ 1	⑪ 1
4	⑬	⑬	⑨ 2	⑪ 1	⑨ 1 2•	⑨ 2	⑦ 3	⑦ 3
5	⑬	⑬	⑪ 1	[12] 1•	[12] 1•	[12] 1•	[12] 1•	[12] 1•
6	⑬	⑪ 1	⑪ 1	⑪ 1	⑪ 1	⑦ 3	[12] 1•	[12] 1•
7	⑬	⑬	[12] 1•	[12] 1•	[12] 1•	[12] 1•	[12] 1•	[12] 1•

	0.1	0.3	0.5	0.7	0.9	1.1	1.3	1.5
0	⑬	⑬	⑪ 1	⑦ 2 2•	⑦ 3	⑨ 2	⑦ 3	⑤ 4
1	⑬	⑪ 1	⑪ 1	⑦ 3	⑦ 3	⑦ 3	⑦ 3	⑤ 3 2•
2	⑬	⑬	⑪ 1	⑨ 2	⑪ 1	⑨ 2	⑦ 3	⑦ 3
3	⑪ 1	⑨ 2	⑪ 1	⑪ 1	⑨ 2	⑨ 1 2•	⑪ 1	⑨ 2
4	⑬	⑪ 1	⑨ 2	⑨ 2	⑨ 1 2•	⑦ 3	⑦ 3	⑦ 3
5	⑬	⑬	⑪ 1	[12] 1•	[12] 1•	[12] 1•	[12] 1•	[12] 1•
6	⑬	⑪ 1	⑪ 1	⑪ 1	⑪ 1	⑦ 3	[12] 1•	[12] 1•
7	⑪ 1	⑪ 1	[12] 1•	[12] 1•	[12] 1•	[12] 1•	[12] 1•	[12] 1•

Fig. 7. One Au on 12 atom cluster collision. The numbers on the left column denote the impact parameter b, measured in Å, and the top row the average energy per atom E in eV. The upper, middle and lower tables correspond to allowing the system to evolve, without heat radiation, for 10^4, 10^6 and 2×10^6 time steps, respectively, before slow quenching during 10^6 additional time steps.

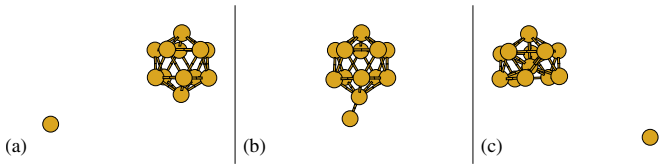

Fig. 8. Collision between a single gold atom and a 12 atom cluster. The single atom approaches the cluster from the left (a), and exchanges energy (b). Finally, in (c) one of the cluster atoms is displaced towards the target center, while the projectile continues along its trajectory.

$0.9 \leq E \leq 1.5$ eV, keeping the impact parameter fixed, coalescence is observed for a few cases, while more often 11 atom clusters, and one dimer are generated. For larger impact parameters, $4 \leq b \leq 7$ Å, fusion is present in the low energy region, but in a few cases target and projectile remain unaltered. Finally, for large b and E values we observe a few cases of coalescence, some 11 atom clusters plus a dimer and many instances of scattering (denoted by squares) in which projectile and target size do not change.

A particularly interesting scattering process, illustrated in Figures 8, occurs for an impact parameter of 5 Å and energies $0.7 < E < 1.1$ eV. When the projectile approaches the target (Fig. 8a) it attracts the nearest (lowest in Fig. 8b) atom, but without removing it from the cluster. This generates a large energy transfer, which in turn induces large amplitude vibrations in the "lowest" atom, as the projectile leaves the scene (Fig. 8c). As a consequence of these large amplitude vibrations this particular atom does overcome the energy barrier and ends up at the center of the cluster (Fig. 8c). Quite remarkably this lower symmetry cluster has an energy slightly smaller than the fully symmetric 12 atom cluster we accepted above as the stable configuration.

In fact, the original $12(\mathrm{I}_h)$ cluster has a binding energy $E_b = -3.03$ eV, while the energy of the less symmetric configuration $12(\mathrm{C}_{5v})$ equals $E_b = -3.09$ eV, which is 2% lower. Thus, we are faced with the question of why this lower energy configuration was not obtained in the minimization process we reported above. The explanation of this apparent contradiction is related to the fact that the energy barrier the atom has to overcome, to shift to the center of the cluster, is rather large and cannot be achieved in a minimization process that starts with an icosahedron and allows only small displacements from the original equilibrium positions. We have developed a genetic algorithm code [63], which allows to look into this matter, and checked that in fact the less symmetric configuration $12(\mathrm{C}_{5v})$ is lower in energy. It is also worth mentioning that this asymmetric structure was assigned minimum energy by WJ [22] as well. However, they argue that the bond compression of the $12(\mathrm{C}_{5v})$ structure generates a repulsion strong enough to destabilize it in favor of the icosahedron.

In the middle and lower illustrations of Figure 7 we display the results of allowing the system to relax at constant cluster temperature for 10^6 and 2×10^6 time steps, respectively, *before* cooling by radiation during an additional 10^6 time steps. The similarities and differences with the upper table are quite apparent. While the low energy and the larger impact parameter collisions are hardly modified, it is observed that the larger the time allowed before slow quenching the stronger the tendency to form dimers. If fragmentation is the dominant cluster cooling mechanism, then the main conclusion one can draw is that mostly dimers will be generated in low impact parameter collisions. On the contrary, if heat radiation dominates then larger, energetically more favorable, configurations will result.

One atom on 13. When a Au atom collides with the "magic number" $N = 13$ cluster the results are not much different from the previous 1 on 12 case. However, there is a larger number of fusion cases, many instances of dimer formation, and also instances are observed where there is no change in the number of atoms of projectile and target. For example, when $E = 0.9$ eV, there is fusion for $b \leq 2$, dimer plus a 12 atom cluster generation for $b = 3$, fusion for $b = 4$, no change $b = 5$, and fusion for $b = 6$ and $b = 7$ Å.

One atom on 14. In this case the results fall into only two categories: either target and projectile fuse or they simply scatter. Fusion prevails for values of $b \leq 5$ Å. For $b > 5$ Å there is coalescence only for very small energies $E \leq 0.3$, and no change in the number of atoms in projectile and target for larger energies. This small b large E behavior can be understood as follows: for low impact parameter the collision gives rise to violent cluster vibrations and deformations, which precludes the trapping of the projectile. Instead, larger b values induce less drastic cluster deformations and sufficient attraction to fuse projectile and target.

One atom on 12: cluster rotation. In all the preceding cases the cluster symmetry axis was taken to be parallel to the y-axis, that is, perpendicular to the initial projectile velocity. Now we align the cluster symmetry axis parallel to the y-axis. A qualitative change is observed: single atoms as a result of the collision. In fact, for low energies and small b there is fusion. However, for $E > 0.7$ eV several alternatives are observed: either coalescence, or 8, 9 and 11 atom cluster formation accompanied by the creation of dimers and single atoms. When $b > 3$ Å we obtain 11 atom clusters plus a dimer or a pair of isolated atoms. Finally, for the largest $b = 7$ Å value no atomic reordering is observed. However, we notice that in general the overall structure of the results is equivalent to the perpendicularly oriented cluster impact discussed above, which allows us to concentrate on cluster collisions without paying much attention to their relative spatial orientation.

3.4 Collisions between two Au clusters

Now we turn to the problem of the collision of two clusters of a few, but in general different, number of atoms.

One dimer on a 12 atom cluster. Fusion is obtained for low energies ($E \leq 0.7$ eV) and for practically all values of the impact parameter b. In many instances the

end result is a dimer and a 12 atom cluster, which are the outcome of a complex dynamic interaction that, finally, yields a reconstruction into the two original clusters. For $E > 0.7$ eV and small b we notice a diversity of results: single atoms plus clusters of 5, 6, 7, 8, 10 and 11 atoms are obtained, which reflects the fact that the more complex the projectile the richer the variety of collision fragments.

One 12 atom cluster on another 12 atom cluster. Fusion is observed only for low energies ($E = 0.1$ eV per atom) over the whole range of impact parameters $0 \leq b \leq 7$ Å. For large energies and small impact parameter collisions, either large fragments plus a couple of dimers or trimers, or dimers and single atoms are generated. For large E and large b, collisions without cluster size rearrangement are predominant.

One 13 atom cluster on a 12 atom cluster. Again there is coalescence for $E \sim 0.1$ eV and $0 \leq b \leq 7$ Å, while for large E and large b collisions without rearrangement predominate. In the $0 \leq b \leq 5$ Å and $E \geq 0.5$ eV region large and medium size fragments plus trimers, dimers and single atoms are produced. Total break up of the cluster is seen almost exclusively for small b and large E collisions.

One 14 atom cluster on a 12 atom cluster. Again here the results are quite similar to the previous ones. For small b there is fusion, while for large b and large E the collision does not modify the size of the colliding clusters. Moreover, in a large region of parameter space ($0 \leq b \leq 5$ Å and $0.5 \leq E \leq 1.5$ eV) a whole variety of fragments does result: large fragments plus dimers, medium size fragments and finally, for the largest energies, total cluster breakup into small pieces.

One 13 atom cluster on a 13 atom cluster. The collision of two "magic number" clusters yields the rich variety of results illustrated in the upper table of Figure 9. It is readily noticed that there are many notable exceptions to the general trends observed in the preceding cases, and which are only present for this particular one. This is specially noticeable in the upper right of the figure, which illustrates the parameter values for which the clusters fragment into dimers, trimers and clusters of 4 to 14, 18, 20, 21 and 24 atoms. However, again fusion is observed for low energy collisions ($E \sim 0.1$ eV) and for all b values, as well as scattering collisions for large impact parameters, which are the final outcome of a complex dynamic process that, in the end, yields a reconstruction into two clusters with the same number of atoms as before the collision.

The middle and lower tables of Figure 9 correspond to keeping the cluster temperature constant for 10^6 and $2{\times}10^6$ time steps, respectively, *before* cooling. They reflect the same general trends already mentioned in relation to Figure 7, i.e. that the larger the time that elapses before slow quenching, the stronger the tendency to form smaller fragments, in particular dimers.

One 14 atom cluster on a 13 atom cluster. A low energy coalescence region, as well as a large impact parameter zone, where after the collision projectile and target rearrange into their original structures, is again obtained. Also, and just as in previous cases, for large E and small b a diversity of fragments (dimers, trimers, and 5 to

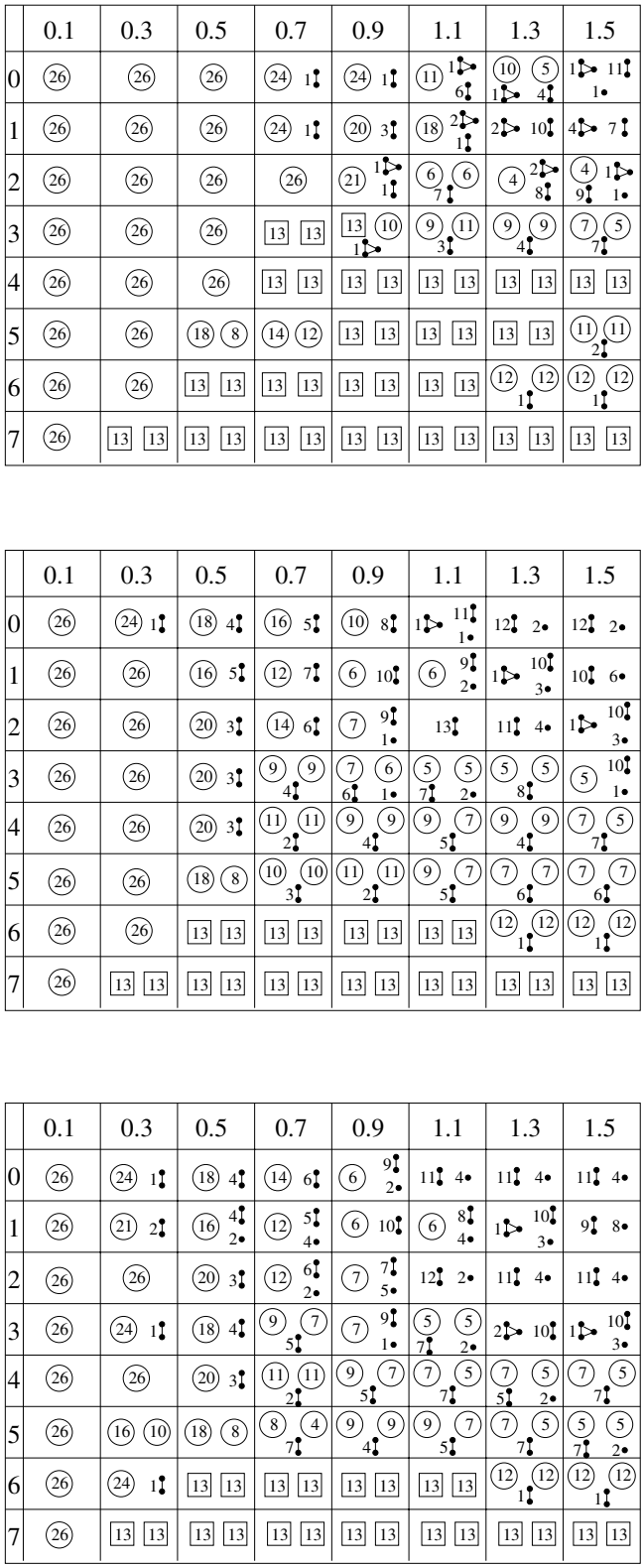

Fig. 9. Collision between two 13 atom clusters. The numbers on the left column denote the impact parameter b, measured in Å, and the top row the average energy per atom E in eV. The upper, middle and lower tables correspond to allowing the system to evolve, without heat radiation, for 10^4, 10^6 and 2×10^6 time steps, respectively, before slow quenching during 10^6 additional time steps.

9 atom clusters) does result. In addition there are several cases with a single Au atom exchange between projectile and cluster, such that the original (14, 13) pair is converted into a (15, 12) one. However, in this same b and E region when three, instead of two, collision fragments are generated, always a dimer (and not a single atom) is created. This dimer originates in the 14 atom projectile, yielding in the end a 12 and a 13 atom cluster plus a dimer, as collision fragments.

4 Conclusions

The dynamics of the collision process of neutral gold clusters has been investigated by means of classical molecular dynamics in combination with embedded atom (EA) potentials. First, the reliability of the EA potentials was confirmed by comparison with ab initio values, finding that EA is in good agreement for the cluster sizes we considered, an agreement which improves as N increases. Next, structural characteristics and the symmetry of the various Au clusters were obtained and contrasted with published results [22].

Several type collisions were investigated, finding regions of fusion, fragmentation and scattering, a behavior that parallels the results of Rohmund et al. [38] for $C_{60}^{+} + C_{60}$ collisions. Which of these outcomes actually occurs depends mainly on the values of the projectile energy E, the impact parameter b and the cluster cooling speed. Fusion is dominant for low energies ($E < 0.7$ eV) and small impact parameters ($b < 3$ Å). Simple scattering, with no change in the size and structure of the colliding clusters, prevails for large E and b values. For large energies and small impact parameters fragmentation and scattering are generally the case. For large E and large b scattering is the most probable outcome. When the cluster does breaks up the main collision products, apart from large fragments, are dimers. The amount of dimers that are generated depends strongly on the speed with which the clusters cool down after colliding. Slow cooling implies that fragmentation is the dominant channel, with the consequent large amount of small fragments, mainly dimers. Faster cooling rates allow the energetically more favorable larger clusters to prevail. On the other hand, cluster coalescence provides a viable mechanism to generate larger cluster sizes. It is also of interest that the collisions themselves turn out to be rather insensitive to the relative orientation of the projectile and target main symmetry axes, and that cluster collisions can generate metastable structures, usually not accessible due to the presence of a potential barrier.

AHR gratefully acknowledges the National Supercomputer Initiative at IPICYT.

References

1. M. Valden, X. Lai, D.W. Goodman, Science **281**, 1647 (1998)
2. W.A. de Heer, Rev. Mod. Phys. **65**, 611 (1993)
3. C.L. Cleveland, U. Landman, T.G. Schaaff, M.N. Shafigullin, P.W. Stephens, R.L. Whetten, Phys. Rev. Lett. **79**, 1873 (1997)
4. T.G. Schaaff, W.G. Cullen, P.N. First, I. Vezmar, R.L. Whetten, C. Gutiérrez-Wing, J. Ascencio, M.J. José-Yacamán, J. Phys. Chem. **101**, 7885 (1997)
5. K.J. Taylor, C.L. Pettiette-Hall, O. Cheshnovsky, R.E. Smalley, J. Chem. Phys. **96**, 3319 (1992)
6. K. Koga, H. Takeo, T. Ikeda, K.I. Ohshima, Phys. Rev. B **57**, 4053 (1998)
7. V.A. Spasov, Y. Shi, K.M. Ervin, Chem. Phys. **262**, 75 (2000)
8. B. Palpant, B. Prevel, J. Lerme, E. Cottancin, M. Pellarin, M. Treilleux, A. Perez, J.L. Vialle, M Broyer, Phys. Rev. B **57**, 1963 (1998)
9. R.L. Whetten, J.T. Khoury, M.M. Alvarez, S. Murthy, I. Vez-mar, Z.L. Wang, P.W. Stephens, C.L. Cleveland, W. D. Luedtke, U. Landman, Adv. Mater. **5**, 8 (1996)
10. R.P. Andres, T. Bein, M. Dorogi, S. Feng, J.I. Henderson, C.P. Kubiank, W. Mahoney, R.G. Osifchin, R. Reifenberger, Science **272**, 1323 (1996)
11. C.A. Mirkin, R.L. Letsinger, R.C. Mucic, J. Storhoff, Nature **382**, 607 (1996)
12. A.P. Alivisatos, K.P. Johnsson, X. Peng, T.E. Wilson, C.J. Loweth, M.P. Bruchez, P.G. Schultz, Nature **382**, 609 (1996)
13. J.J. Zhao, X.S. Chen, G.H. Wang, Phys. Lett. A**189**, 223 (1994)
14. H. Handschuh, G. Ganteför, P.S. Becthold, W. Eberhart, J. Chem. Phys. **100**, 7093 (1994)
15. I.L. Garzon, A. Posada-Amarilla, Phys. Rev. B**54**, 11796 (1996)
16. O.D. Häberlen, S.C. Chung, M. Stener, N. Rösch, J. Chem. Phys. **106**, 5189 (1997)
17. J. Wang, G. Wang, J. Zhao, Phys. Rev. B**66**, 035418 (2002)
18. I.L. Garzon, K. Michaelian, M.R. Beltran, A. Posada-Amarilla, P. Ordejón, E. Artacho, D. Sánchez-Portal, J.M. Soler, Phys Rev Lett. **81**, 1600 (1998)
19. J.L. BelBruno, Heteroatom. Chem. **9**, 651 (1998)
20. R.N. Barnett, C.L. Cleveland, H. Häkkinen, W.D. Luedtke, C. Yannouleas, U. Landman, Eur. Phys. J. D **9**, 95 (1999)
21. J.M. Soler, M.R. Beltran, K. Michaelian, I.L. Garzon, P. Ordejón, D. Sánchez-Portal, E. Artacho, Phys. Rev. B **61**, 5771 (2000)
22. N.T. Wilson, R.L. Johnston, Eur. Phys. J. D **12**, 161 (2000)
23. T. Li, S. Yin, Y. Ji, G. Wang, J. Zhao, Phys. Lett. A **267**, 403 (2000)
24. H. Häkkinen, U. Landman, Phys. Rev. B **62**, 2287 (2000)
25. H. Grönbech, W. Andreoni, Chem. Phys. **262**, 1 (2000)
26. A.H. Romero, A. Castro, A. Rubio, to be published
27. J. Li, X. Li, H.-J. Zhai, L.-S. Wang, Science **299**, 864 (2003)
28. N. Andersen, J.W. Gallagher, I.V. Hertel, Phys. Rep. **278**, 165 (1988)
29. N. Andersen, J.T. Broad, E.E.B. Campbell, J.W. Gallagher, I.V. Hertel, Phys. Rep. **278**, 107 (1997)
30. N. Andersen, K. Bartschat, J.T. Broad, I.V. Hertel, Phys. Rep. **279**, 251 (1997)
31. R. Schmidt, G. Seifert, H.O. Lutz, Phys. Lett. A **158**, 231 (1991)

32. G. Seifert , R. Schmidt, H.O. Lutz, Phys. Lett. A **158**, 237 (1991)
33. O. Knospe, R. Schmidt, E. Engel, U.R. Schmitt, R.M. Dreizler, H.O. Lutz, Phys. Lett. A **183**, 332 (1993)
34. F.S. Zhang, F. Spiegelmann, E. Suraud, V. Frayssé, R. Poteau, R. Glowinski, F. Chatelin, Phys. Lett. A **193**, 75 (1994)
35. R. Schmidt, H.O. Lutz, Phys. Lett. A **183**, 338 (1993)
36. R. Schmidt, H.O. Lutz, Phys. Rev. A **45**, 7981338 (1992)
37. A.M. Mazzone, Nucl. Inst. Meth. Phys. Res. B **142**, 17 (1998)
38. F. Rohmund, E.B. Campbell, O. Knospe, G. Seifert, R. Schmidt, Phys. Rev. Lett. **76**, 3289 (1996)
39. E.E.B. Campbell, A.V. Glotov, A. Lassesson, R.D. Levine, C. R. Phys. **3**, 341 (2002)
40. M. Vogel, K. Hansen, A. Herlert, L. Schweikhard, Phys. Rev. Lett. **87**, 013401 (2001)
41. M. Vogel, K. Hansen, A. Herlert, L. Schweikhard, J. Phys. B**36**, 1073 (2003)
42. M.W. Mathews, R.J. Beuhler, M. Ledbetter, L. Friedman, J. Phys. Chem. **90**, 251 (1986)
43. P.M. Echeñique, J.R. Manson, R.H. Ritchie, Phys. Rev. Lett. **64**, 1413 (1990)
44. M.H. Shapiro, T.A. Tombrello, Phys. Rev. Lett. **65**, 92 (1990)
45. M.H. Shapiro, T.A. Tombrello, Nucl. Inst. Meth. **58**, 161 (1991)
46. E. Blastein-Barojas, M.R. Zachariah, Phys. Rev. B **45**, 4403 (1992)
47. A. Glotov, R. Schmidt, E.B. Campbell, Eur. Phys. J. D **16**, 333 (2001)
48. R. Car, M. Parrinello, Phys. Rev. Lett. **55**, 2471 (1985); we have used the CPMD code, version 3.5, developed by J. Hutter et al., at MPI für Festkörperforschung and IBM Research Laboratory (1990-2001)
49. J.P. Perdew, K. Burke, M. Ernzerhof, Phys. Rev. Lett. **175**, 531 (1990)
50. H. Partridge, C.W. Bauschlicher, S.R. Langhoff, Chem. Phys. Lett. **175**, 531 (1990)
51. J.M. Seminario, J.M. Tour, Int. J. Quant. Chem. **65**, 749 (1997)
52. J. Rogan, A.H. Romero, R. Ramírez, M. Kiwi, to be published.
53. N. Troullier, J. Martins, Phys. Rev. B **43**, 1993 (1991)
54. M.S. Daw, M.I. Baskes, Phys. Rev. B **29**, 6443 (1984)
55. S.M. Foiles, M.I. Baskes, M.S. Daw, Phys. Rev. B **33**, 7983 (1986)
56. J.N. Murrell, R.E. Mottram, Mol. Phys. **69**, 571 (1990)
57. H. Cox, R.L. Johnston, J.N. Murrell, J. Sol. State Chem. **145**, 517 (1999) and references therein
58. C. Walther et al., Chem. Phys. Lett. **256**, 77 (1996)
59. L.S. Kassel, J. Phys. Chem. **32**, 225 (1928)
60. O.K. Rice, H.C. Rampsperger, J. Am. Chem. Soc. **50**, 6617 (1928)
61. R.A. Marcus, J. Phys. Chem. **20**, 359 (1952)
62. V. Weisskopf, Phys. Rev. **52**, 295 (1937)
63. A.H. Romero, R. Ramírez, J. Rogan, M. Kiwi, to be published